Numerical modelling of oblique shock and detonation waves induced in a wedged channel

H Y Fan and **F K Lu***
Aerodynamics Research Centre, Department of Mechanical and Aerospace Engineering, University of Texas at Arlington, Arlington, Texas, USA

The manuscript was received on 3 August 2007 and was accepted after revision for publication on 14 February 2008.

DOI: 10.1243/09544100JAERO273

Abstract: A computational study of wedge-induced oblique shock and detonation wave phenomena in the flow of a combustible mixture over a wedged channel is presented with the purpose of understanding the fundamental gasdynamics of the waves and their interactions. A two-dimensional, time accurate, finite-volume-based method was used to perform the computations, and a five-species, two-step chemical reaction is assumed for a stoichiometric hydrogen–air mixture. The combustion channel is made of a wedged section followed by a constant area section. The simulation was performed with wedges of up to 20° semi-angle and Mach numbers from 1.25 to 6, with other inflow parameters fixed. Within the computational domain either propagating or standing shock and detonation wave configurations were obtained depending on the flow Mach number and the wedge semi-angle. Four flow modes, namely, a propagating detonation wave, a standing detonation wave, a propagating shock wave, and a standing shock wave mode were identified. The two detonation-based modes were emphasized. Detonation initiation, propagation, and the induced wave interactions of these modes were investigated. The shock-based modes were also studied briefly. Phenomena explored included overall wave structures, detonation initiation arising from shock coalescence, location of initiation, and double detonation initiation. The physical mechanisms of these phenomena were analysed.

Keywords: detonation, shock wave, reactive flow, wedged channel

1 INTRODUCTION

Oblique shock theory indicates that the supersonic flow of a perfect gas with a specific heat ratio of γ past a sharp wedge at zero incidence is governed by the incoming Mach number M_1 and the wedge semi-angle θ. For semi-angles below a maximum value, the theory admits a weak and a strong solution. The strong solution is unrealizable physically. The weak solution comprises an oblique shock inclined at an angle β to the incoming stream. When the wedge angle equals $\theta_{\max}$, a sonic condition exists downstream of the shock. When θ exceeds $\theta_{\max}$, there is no attached shock solution. Instead, a curved bow shock forms upstream of the wedge. The value of $\theta_{\max}$ is a function of M_1 for a given perfect gas. When an attached shock solution is available, there is conical symmetry in that there is no geometric lengthscale.

Beyond the simple configuration described above, one can construct more complicated ones, such as a double wedge or a wedge expansion. These configurations introduce a geometric lengthscale that seriously affect the flow downstream. For example, the compound wedge produces shock–shock interactions that depend on the second wedge angle θ_2, as described in reference [**1**]. A further complication arises if the wedge is placed in the middle of a channel, as may be found in scramjet modules with sidewall or two-dimensional compression surfaces, where multiple wave interactions occur [**2–4**]. For a sufficiently large value of M_1 which admits an attached shock solution, the subsequent shock reflections eventually result in a flow Mach number that cannot turn the flow through θ. A curved, terminal shock

Corresponding author: Aerodynamics Research Centre, Department of Mechanical and Aerospace Engineering, University of Texas at Arlington, 214B Woolf Hall, 500 West 1st Street, P. O. Box 19018, Arlington, TX 76019-0018, USA. email: franklu@uta.edu

forms when this happens. The downstream flow then becomes subsonic. Subsequently, downstream disturbances can cause flow instability that 'pop' the shock system forwards, past the wedge to result in a bow shock configuration, a phenomenon known as 'inlet unstart' in high-speed propulsion. Should the wedge be short, that is, should it terminate at a shoulder parallel to the incoming flow, the above phenomenon still exists.

If the incoming flow is that of a supersonic combustible mixture as, for example, in certain proposed detonation-based propulsion systems [**5–8**], the shock may induce combustion, depending on the mixture composition, and flow and geometric parameters. Possibilities of deflagration or detonation or post-shock stability arise. To address these issues, a comprehensive numerical study of a confined wedge in a supersonic, combustible flow was performed. To capture the essential physics, two-dimensional Euler computations were performed to avoid the complications of transport properties. The chemical reaction for a stoichiometric $H_2/O_2/N_2$ flow is described by a simple two-step reaction involving five species: H_2, O_2, N_2, H_2O, and OH. The code that was used included a two-temperature model for vibrational non-equilibrium, but this effect was found to be negligibly small. The computations, nonetheless, were performed with the non-equilibrium model kept intact.

1.1 Literature review

Wedge- and cone-induced oblique shock and detonation waves have recently received attention due to their potential application in hypersonic propulsion devices. These include ram accelerators (see e.g. [**9–11**]) and oblique detonation wave engines (ODWEs) [**12–14**].

Experimental observations of oblique shock-induced detonation [**15–20**] have shown that there are at least two different types of flow that can arise. The first is a direct initiation of a detonation wave within a stagnation region. The second is an oblique shock wave that transitions to an oblique detonation wave a certain distance from the wedge's leading edge.

Numerical simulation of wedge- and cone-induced detonation has been done in the recent past [**9**, **12**, **21–30**]. These studies were concerned with the body in a semi-infinite domain. Generally, the studies showed two possible ways in which a detonation is achieved. In the first, an attached oblique shock in the incoming premixed combustible mixture transitions to a detonation, arising from the compression. In the second, a direct initiation is obtained. Under certain conditions, a stable wave system is not achieved.

A wedge confined in a channel and the induced complex wave interactions appear to be a realistic model to the flow of a ram accelerator or an ODWE. In this situation, the extra compression from multiple shock reflections is expected to trigger detonation. The multiple oblique wave reflections eventually terminate with subsonic outflow. When this happens, an unstable wave system arises, with the detonation wave propagating upstream. This unstable detonation mode has been proposed as a possible propulsion technique for high-speed flight [**6**, **7**]. The intrinsic unsteadiness of the confined detonation flow is the subject of the present study.

2 METHOD

2.1 Model equations and numerical considerations

The numerical technique was previously reported by Kim *et al.* [**31**] and only a brief overview is provided here. The time-dependent, two-dimensional, Euler equations are used to describe an inviscid, non-heat-conducting, reacting gas flow in which thermal non-equilibrium is modelled with a two-temperature model. These equations can be expressed in Cartesian coordinates as

$$\frac{\partial \boldsymbol{U}}{\partial t} + \frac{\partial \boldsymbol{F}}{\partial x} + \frac{\partial \boldsymbol{G}}{\partial y} = \boldsymbol{S} \tag{1}$$

where $\boldsymbol{U}$ is the vector of conserved variables, $\boldsymbol{F}$ and $\boldsymbol{G}$ are the convective flux vectors, and $\boldsymbol{S}$ the vector of source terms

$$\boldsymbol{U} = \begin{bmatrix} \rho_s \\ \rho u \\ \rho v \\ \rho e_{\mathrm{v}} \\ \rho E \end{bmatrix}, \quad \boldsymbol{F} = \begin{bmatrix} \rho_s u \\ \rho u^2 + p \\ \rho uv \\ \rho u e_{\mathrm{v}} \\ \rho uE + pu \end{bmatrix}, \quad \boldsymbol{G} = \begin{bmatrix} \rho_s v \\ \rho uv \\ \rho v^2 + p \\ \rho v e_{\mathrm{v}} \\ \rho vE + pv \end{bmatrix},$$

$$\boldsymbol{S} = \begin{bmatrix} w_s \\ 0 \\ 0 \\ w_{\mathrm{v}} \\ 0 \end{bmatrix} \tag{2}$$

The subscript $s = 1, 2, 3, \ldots, N_s$ where N_s is the number of species. The first N_s rows represent species continuity, followed by the two momentum conservation equations for the mixture. The next row describes the rate of change in the vibrational energy and the final row is the total energy conservation equation. The terms u and v are the velocities in the x and y directions, respectively, $\rho = \sum_{s=1}^{N_s} \rho_s$ is the mixture density, ρ_s is the density of species s, p is the pressure, e_{v} is the vibrational energy, E is the total energy per unit mass of mixture, w_s is the mass of production rate of species s per unit volume, and w_{v} is the vibrational energy source.

The internal energy based on the two-temperature model is assumed to comprise an equilibrium portion at the translational temperature T and a non-equilibrium portion at the vibrational temperature T_v, and can be defined as

$$e = e_{eq}(T) + e_v(T_v) \tag{3}$$

These energy components can be determined with certain thermodynamic relations.

The source terms for the species mass production rate in the chemical reactions can be written as

$$w_s = M_s \sum_{r=1}^{N_r} (\beta_{s,r} - \alpha_{s,r})(R_{f,r} - R_{b,r}) \tag{4}$$

where M_s is the molecular weight of species s, N_r the number of reactions, $\alpha_{s,r}$ and $\beta_{s,r}$ are the stoichiometric coefficients for reactants and products, respectively, in the rth reaction. The forward and backward reaction rates of the rth reaction are $R_{f,r}$ and $R_{b,r}$, respectively. These rates can be determined by the Arrhenius law.

The source term of vibrational energy can be written as

$$w_v = \sum_s Q_{v,s} + \sum_s w_s e_{v,s} \tag{5}$$

The first term on the right-hand side, $Q_{v,s}$, represents the vibrational energy exchange rate of species s due to the relaxation process with translational energy, which can be determined by the Landau–Teller formulation [**32**, **33**]. The second term, $w_s e_{v,s}$, represents the amount of vibrational energy gained or lost due to production or depletion of species s from chemical reactions.

A finite-volume algorithm is used to solve these equations numerically. The advantage of this method is its use of the integral form of the equations, which ensures conservation and that allows for the correct treatment of discontinuities. Non-equilibrium flow involving finite-rate chemistry and thermal energy relaxation often can be very difficult to solve numerically because of stiffness. The present method includes a point implicit treatment of source terms to reduce the inherent stiffness of the system by effectively rescaling all the characteristic times in the fields into the same order of magnitude. A 'local ignition averaging model' (LIAM) [**31**] is further taken to handle the additional stiffness in the ignition cells. The basic idea for this model comes from the fact that the species mass fractions are changing drastically in a very short period when the reactants are ignited but reaches equilibrium soon afterwards. LIAM separates the cell in which the ignition condition is met and then integrates the chemical kinetics equations alone in that cell with a time step much smaller than the flow solver time step. Temporal accuracy is improved by using a two-step explicit Runge–Kutta time integration scheme instead of first-order accurate Euler integration. Moreover, Roe's flux-difference split scheme is implemented for the cell interface fluxes, and a monotone upstream-centred schemes for conservation laws extrapolation approach is further combined for a high spatial accuracy. The method hereby yields second-order accurate results in both space and time at smooth parts of the flow, while it still keeps first-order accuracy at discontinuities as shock waves.

In the present study, the Rogers–Chinitz [**34**] hydrogen–air combustion mechanism of five species (N_2, O_2, H_2, H_2O, and OH) and two reactions ($H_2 + O_2 = 2OH$ and $2OH + H_2 = 2H_2O$) is used. This model was developed to represent hydrogen–air chemical kinetics with as few reaction steps as possible while still giving reasonably accurate global results. In this model, nitrogen is counted as a collisional partner in the thermodynamic model and relaxation process, but not included in the chemical reaction model since the maximum temperature in the hydrogen–air reaction does not reach the dissociation temperature of nitrogen. The previous work by Kim *et al.* [**31**] demonstrated that this simplified reaction mechanism together with the solution strategies discussed above can handle the stiffness in time caused by the reaction and accurately represent the physical system.

2.2 Geometric configuration and flow conditions

The wedged channel geometry is shown in Fig. 1. The two-dimensional channel is formed from a symmetric wedge with a straight end-section symmetrically arranged within a straight chamber. The wedge semi-angle θ ranges from 2.5 to 20°. The sharp wedge, pointing upstream, is 60 mm wide and is attached to an aftbody, 100 mm long, and of the same width as the base of the wedge. The entire channel is 100 mm wide. The upper half of the wedged channel is taken as the computation domain. The length of the computational domain varies from 300 through 800 mm

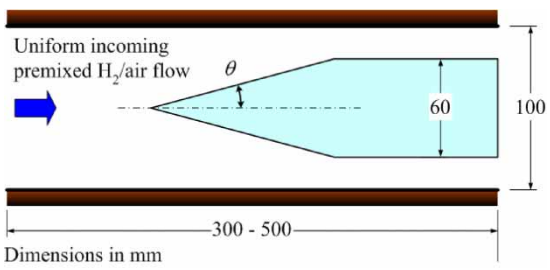

Fig. 1 Schematic of the wedged channel configuration

depending on θ. This variation ensures that the clearance between the wedge tip and channel inlet remains sufficient for the simulation.

The incoming supersonic flow comprises a premixed stoichiometric hydrogen–air mixture. The pressure and temperature of the flow are fixed at $p_1 = 0.1$ MPa and $T_1 = 700$ K, respectively, while the incoming Mach number is allowed to vary from 1.25 through 6. The left boundary of the domain is kept at the inflow conditions. At the outflow boundary, non-reflective characteristic boundary conditions are implemented. Computations were performed only on the upper half of the configuration due to the geometric symmetry. Slip conditions are imposed at the surfaces of the wedge, aftbody and the confined channel. The different parts of the computational domain are meshed with structured grids, which are not all identical. The minimum and maximum grid spacings used in the present study are 0.4 and 1.0 mm, respectively. A mesh convergence study by Kim *et al.* [**31**] showed that these grid sizes can well handle the problems to be modelled spatially. A similar mesh convergence test done by Lu *et al.* [**35**] in a related work also showed that a maximum grid spacing of 1.0 mm can capture the detonation waves. It has to be noted, however, that such a grid scale may be too coarse to resolve the finer spatial detonation features. For example, an important characteristic that needs to be resolved is the induction layer, a very small zone with no heat release between the shock front and the following reaction zone. To analytically estimate the smallest lengthscale is difficult since it depends on the reaction mechanism and the flow initial conditions. Nevertheless, according to a recent comprehensive numerical study [**36**], it is concluded that for the stoichiometric hydrogen–air mixture in the current study, the induction zone length can be as short as 0.15–0.2 mm. (See also references [**37**] and [**38**] for a review of the spatial resolution requirements of detailed chemistry in detonation modelling.) The above discussion implies that a mesh with maximum grid spacing of less than 0.15 mm is necessary if this layer is to be resolved properly. With the chosen numerical method and the existing computational resource, simulation on such a small mesh size will result in an extraordinarily time-consuming effort. Such an effort may not be worthwhile since the present study focuses on the large-scale features of detonation waves from an applied perspective, such as the behaviour of detonation initiation and propagation, and the induced wave interactions. The selected mesh size is hereby considered to be adequate. The flow solver time step in the simulation is 10^{-7} s, which is typical, and was proved capable of resolving the timescales of interest [**31**, **35**, **39**]. The matrix of test cases is shown in Fig. 2. The figure also shows various flow configuration domains which will be discussed later.

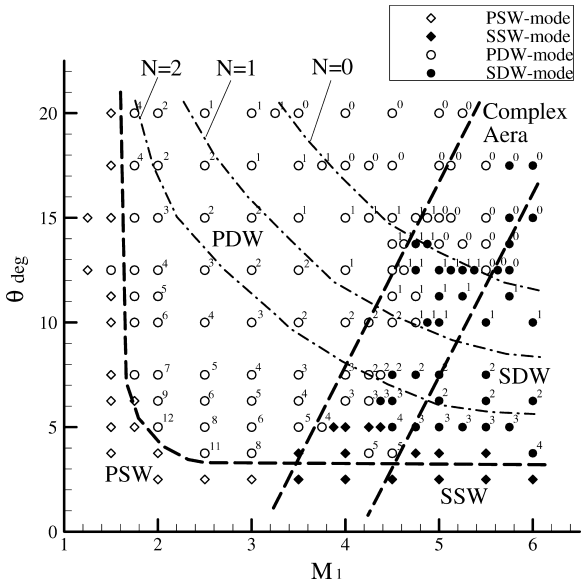

Fig. 2 Matrix of test cases and flow modes

3 RESULTS AND DISCUSSION

Detonation initiation is accompanied by a deflagration-to-detonation transition unless the initiation energy is sufficiently high [**40**]. The previous work using the same numerical technique suggests that a transition phenomenon can be captured [**31**, **35**, **39**]. Though a transition process may appear in some cases, the present simulations show in general that the ignited flow can transit rapidly to the Chapman–Jouguet (CJ) state ($p_{CJ} = 0.665$ MPa, $T_{CJ} = 3014$ K, and $D_{CJ} = 1927$ m/s). The rapid transition in the present simulations supports the experimental observation by Lu and Wilson [**41**] that shock-induced detonation occurs almost instantly and seems to indicate that a direct initiation is possible with shock-induced detonation. In the present study, the discussion is based on the assumption that the combustion rapidly transits to detonation.

Moreover, shock and detonation polar diagrams are provided in the discussion where necessary to assist in interpreting the numerical simulation results obtained in this study. The polar diagrams are obtained from an idealized planar shock or detonation wave analysis assuming that the specific heat ratio is constant. The shock polar technique for a perfect gas is well described in gasdynamics texts (see e.g. [**42**]). The detonation polar diagrams used in the discussion are determined assuming that the heat release after the detonation front is constant, and that the heat release can be evaluated from the numerical simulation results of the related cases. Details of the detonation polar technique can be found in reference [**43**].

3.1 Typical modes

Within the computational domain, either propagating or standing shock and detonation wave configurations are obtained depending on the flow incoming Mach number M_1 and the wedge semi-angle θ. Moreover, whether a detonation occurs also depends on the values of M_1 and θ. Consequently, the shock and detonation wave configurations in the wedged channel can be classified into four major modes depending on whether they are propagating or standing and on whether detonation occurs or not. Configurations that yield propagating detonation waves (PDWs) belong to the 'PDW mode'. The other three modes are correspondingly denoted as the 'propagating shock wave (PSW) mode', the 'standing detonation wave (SDW) mode', and the 'standing shock wave (SSW) mode'. These four modes are indicated in Fig. 2.

As can be seen in Fig. 2, the propagating modes are located to the left while the standing modes are located to the right, separated by a complex area. This complex area (bounded approximately by the two straight dashed lines) can be regarded as a transition region because, within that area, propagating and standing modes can occur alternately (for example, see the test points in the region for $\theta = 12.5$–$17.5°$). In Fig. 2, the complex area stretches to the upper right as M_1 and θ increase. This reveals that the larger the wedge semi-angle, the larger the incoming Mach number required to achieve a stabilized wave system. Finally, the boundary separating the detonation mode from the non-detonative (shock) mode is also plotted in Fig. 2 by a curved dashed line. Here, attention is focused on the detonative modes; the non-detonative modes are only briefly discussed.

3.1.1 PDW mode

The PDW mode can be initiated either after multiple oblique shock reflections in the aftbody area or directly at the wedge tip, depending on M_1 and θ, for the given incoming pressure and temperature. In this mode, a detonation wave that is formed following a number of shock reflections propagates upstream because the detonation wave speed is larger than the incoming local flow velocity in the channel. Alternatively, a detonation wave that is formed at the wedge tip can also propagate upstream if the post-wave reflections cause the downstream flow to become subsonic and unstable. In this latter case, downstream subsonic flow allows disturbances to propagate upstream to overtake the original wedge-attached detonation wave, an example of which will be discussed subsequently. There appears to be various ways for initiating and propagating the detonation wave even in this mode. Some of these are discussed with the following three examples.

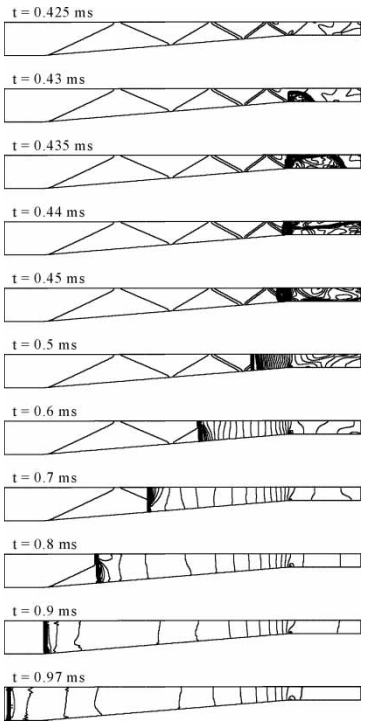

Fig. 3 Evolution of the PDW for $M_1 = 3$ and $\theta = 5°$; example case 1 of the PDW mode

The first example is the case for $M_1 = 3$ and $\theta = 5°$. Figure 3 shows the isobars at various times following the initial establishment of an attached, oblique shock train. At $t = 0.4275$ ms, a detonation kernel is induced over the aftbody, just downstream of the wedge shoulder, after six reflections from the wedge-attached shock. Correspondingly, the shock polar diagram of Fig. 4 shows that at the moment just before the formation of the detonation kernel, the pressure is raised to above the CJ value by six shock reflections (state 7). The detonation kernel grows to fill the entire width of the channel by $t = 0.435$ ms.

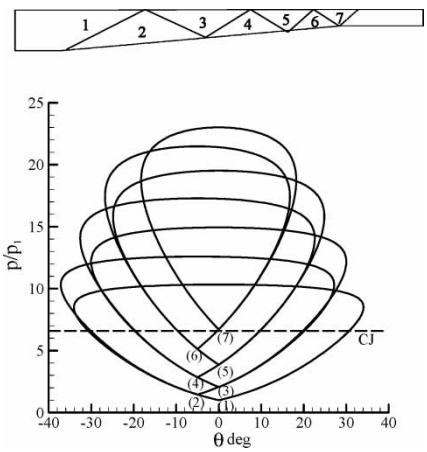

Fig. 4 Polar diagram for $M_1 = 3$ and $\theta = 5°$; example case 1 of the PDW mode

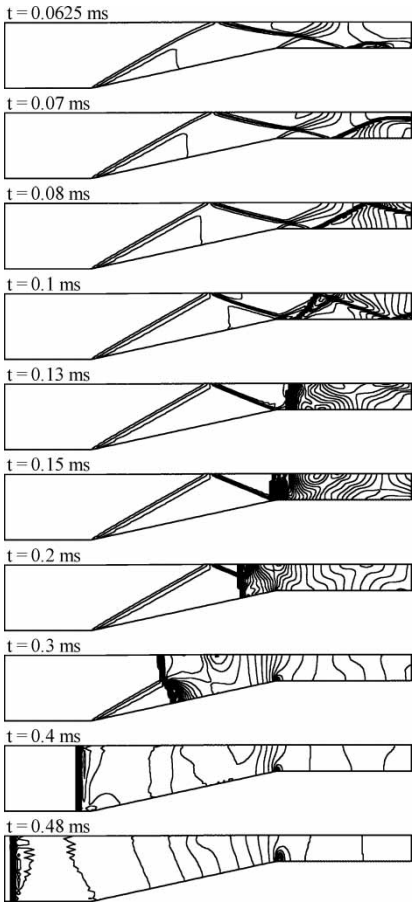

Fig. 5 Evolution of the PDWs for $M_1 = 3.5$ and $\theta = 12.5°$; example case 2 of the PDW mode

The kernel's downstream propagating front is elongated by the incoming flow. However, the upstream front is travelling against the incoming flow and propagates at a slower rate. As this upstream detonation front propagates past the wedge, it encounters and overtakes the steady, oblique shock system. Eventually, this detonation front exits the wedge area, becomes purely normal in the straight inlet channel and propagates out of the left computational boundary.

The next example is for the $M_1 = 3.5$ and $\theta = 12.5°$ case. The evolution of the shock and detonation wave is shown by isobars in Fig. 5. The wedge tip induces an attached shock which is reflected off the channel wall and impinges the aftbody to ignite a detonation kernel, as can be seen by the isobars at $t = 0.0625$ ms. This instant is depicted by the corresponding shock polar in Fig. 6. The polar shows that the flow after two shock reflections (i.e. state 3) attains the CJ pressure. The simulation shows an expansion fan from the wedge shoulder interacting with the reflected wave but the interaction is weak and thus is not considered in constructing the polar. The detonation kernel grows and reaches the opposite wall on which it is reflected. The detonation kernel then evolves into an oblique front at $t =$ 0.08 ms. This oblique front is not stable and propagates

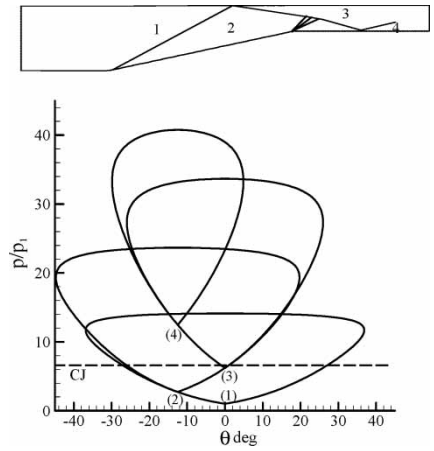

Fig. 6 Polar diagram for $M_1 = 3.5$ and $\theta = 12.5°$; example case 2 of the PDW mode

forward, eventually evolving into a normal front by $t = 0.13$ ms. The detonation wave continues to propagate upstream, overtaking the oblique shocks to enter the inlet until it exits the left computational boundary.

The third example is for $M_1 = 4.5$ and $\theta = 20°$, and is shown by isobars in Fig. 7. This case represents the

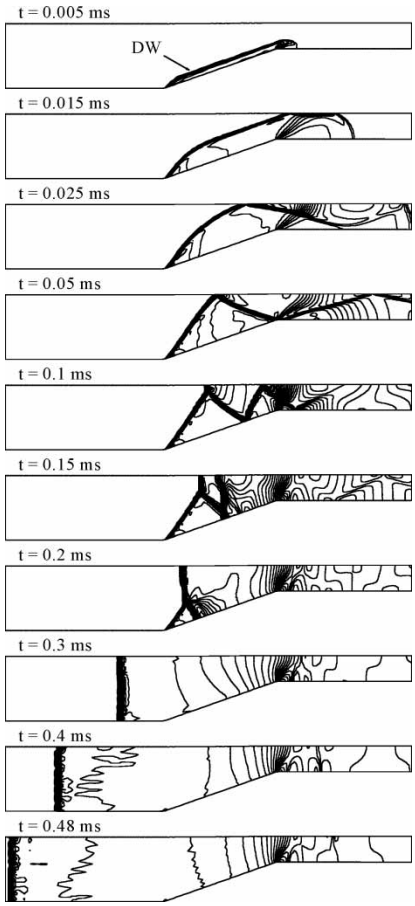

Fig. 7 Evolution of the PDW for $M_1 = 4.5$ and $\theta = 20°$; example case 3 of the PDW mode

strongest wave initiation and interaction among the three examples for the PDW mode. A detonation wave is directly initiated from the wedge tip, as the incoming Mach number is sufficiently large for the wedge that the post-shock parameters exceeds the CJ state and thereby triggers detonation. The numerical results show that detonation is ignited at the very instant that the flow passes the wedge. Figure 7 shows the detonation wave 'DW' already forming at $t = 0.005$ ms. The detonation front that impinges the wedge tip develops promptly to over the whole wedge surface. The detonation front is reflected off the opposite channel wall to induce further shock reflections, which eventually results in a subsonic downstream flow. This then causes the wave system to coalesce and to propagate upstream to overtake the existent oblique detonation front. A new normal front forms and propagates upstream to exit the left computational boundary.

The polar diagram for only the oblique detonation wave and its reflected shock is plotted in Fig. 8. The figure also plots a shock polar with a dash-dotted line assuming an inert flow. Thus, an oblique shock due to a 20° deflection in an inert flow is represented by the path $1' \rightarrow 2'$, whereas the oblique detonation wave due to the same deflection is represented by the wriggly line $1' \rightarrow 2$, indicating obviously that the post-detonation flow exists at a higher state than a post-shock flow. The post-shock inert flow (state 2′) actually raises the pressure to above the CJ value, implying an unstable situation that triggers detonation. This is in accordance with the simulations that detonation is initiated essentially from the moment the flow arrives at the tip of the wedge. The shock polar originating at 2 further suggests that the wedge-induced detonation wave is unable to induce a reflection to yield a uniform downstream flow. This fact is added evidence

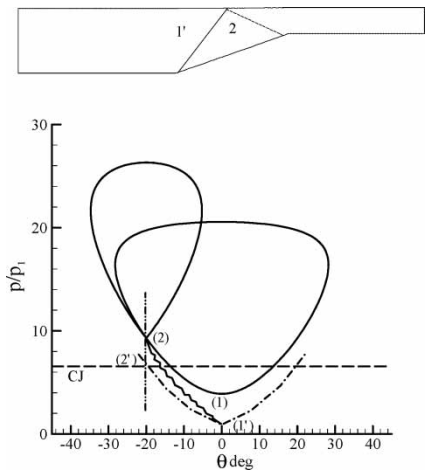

Fig. 8 Polar diagram for $M_1 = 4.5$ and $\theta = 20°$; example case 3 of the PDW mode

of the unsteadiness of this simulated shock and detonation wave configuration. The displacement of the detonation polar above the shock polar (state 1 versus 1′) is due to the pressure rise accompanying the heat release from the detonation.

The pressure distributions on the lower computational boundary on which detonation is initiated are shown in Fig. 9 for the above three PDW examples. Instead of following the actual computational boundary, the abscissa plots the horizontal distance. In the figure, three instants of time from detonation initiation together with a time just before detonation initiation are used to record the pressures for each of the first two cases. Because the third case directly initiates detonation from a very early time, three time instances from detonation initiation are only used to record the corresponding pressure distributions. The results clearly show that the multiple shock reflections result in a narrow, high thermodynamic parameter region where the combustible gaseous mixture reaches the CJ state and begins to detonate. The peak detonation pressures and temperatures are much higher than the CJ state, with the tendency that the peak value increases as M_1 and θ increase. As the detonation wave propagates over the wedge, the second and third cases present an abrupt Taylor expansion after the detonation front whereas the first case presents a gentler expansion behind the detonation front. Furthermore, when the detonation wave moves in the straight inlet area, the flow behind is able to maintain fairly uniform conditions.

3.1.2 SDW mode

A detonation wave can be stabilized by a wedge to achieve an SDW mode if the incoming Mach number is large enough. Basically, the stabilization of the detonation wave depends directly on a balance between the wave propagation rate and the local flow speed. Whether the wave is stable ultimately depends on the two input parameters M_1 and θ. Two stable configurations apparently can be achieved, namely, a normal detonation wave stabilized in the aftbody area or an oblique detonation wave stabilized from the tip of the wedge. A series of wave reflections occur downstream of the detonation wave.

The first example of the SDW mode is for the $M_1 = 5$ and $\theta = 5°$ case. The evolution of the SDW is shown by isobars in Fig. 10. The polar diagram for the shock system before detonation initiation is plotted in Fig. 11. Detonation is initiated after three shock reflections in the aftbody area ($t = 0.1275$ ms) in the tip area of the third oblique shock that impinges the channel surface. The weak expansion waves emanating from the wedge shoulder (4 in Fig. 11) do not affect the detonation initiation significantly. The flow state in 5 before detonation initiation (e.g. pressure) exceeds the CJ value

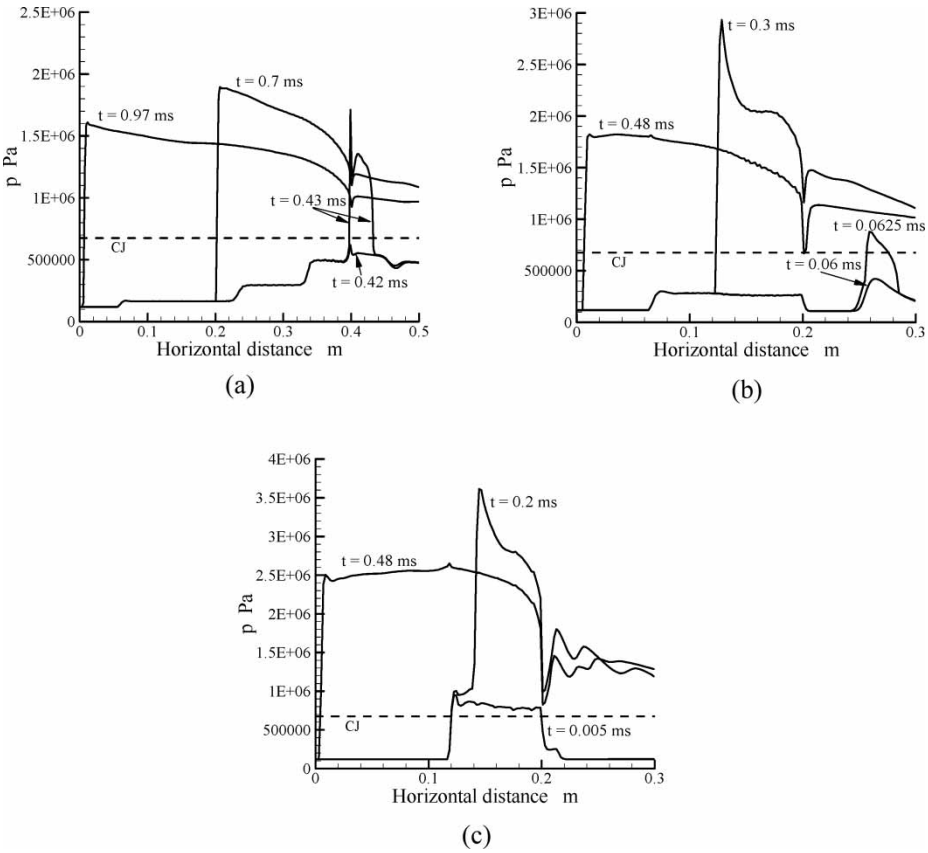

Fig. 9 Pressure distributions on the lower computational boundary for the three example cases of the PDW mode: (a) example case 1: $M_1 = 3, \theta = 5°$; (b) example case 2: $M_1 = 3.5, \theta = 12.5°$; (c) example case 3: $M_1 = 4.5, \theta = 20°$

as shown in the polar of Fig. 12. This ensures shock-initiated detonation. The detonation kernel rapidly enlarges, reflects off the aftbody surface and eventually stabilizes to a detonation front at $t = 0.35$ ms, with a λ-foot structure that will be further discussed later.

The next example is for the $M_1 = 5.5$ and $\theta = 10°$ case. The evolution of the SDW for this case is shown by isobars in Fig. 12. The polar diagram for the shock and detonation system is presented in Fig. 13. To assist in the explanation, the figure also plots the polar for a reflected shock assuming inert flow as a chained line. Detonation is initiated after the attached shock impinges the wall surface in the aftbody area ($t = 0.03$ ms). The actual detonation process proceeds according to $1 \rightarrow 2' \rightarrow 3$. Moreover, the shock polar of Fig. 13 shows that an inert flow would reach state $3'$ with a pressure exceeding the CJ value. Just as in the above case, such a situation is not achieved and a detonation is initiated. The detonation kernel expands rapidly and impinges the opposite aftbody surface to result in an oblique detonation front at about $t = 0.04$ ms. The induced detonation front and the following shock wave structure develop and eventually stabilize after $t = 0.2$ ms.

The final example of the SDW mode is for the $M_1 = 6$ and $\theta = 15°$ case, which is the strongest case of the three discussed. The evolution of the SDW is shown by isobars in Fig. 14. Detonation is directly initiated at the wedge tip. Hence, a very early flow ignition is observed at $t = 0.005$ ms. A detonation wave evolves over the entire wedge surface and is then reflected off the opposite channel wall to form a complete oblique detonation front. Behind the oblique detonation wave is a shock reflection on the wedge. Further shock and expansion interactions and reflections occur in the aftbody area that are finally stabilized after $t = 0.24$ ms. The polar diagram of the detonation wave and the reflected shock are depicted in Fig. 15. Included in the figure is the polar of an attached shock assuming inert flow, shown by a chained line. The results suggest that an inert flow can reach the CJ pressure after passing over the wedge (state $2'$ in Fig. 15), implying that detonation can be directly initiated at the wedge tip, as demonstrated in the simulation.

The pressure distributions at selected times for the above three examples are shown in Fig. 16. The data are recorded on the upper computational boundary for

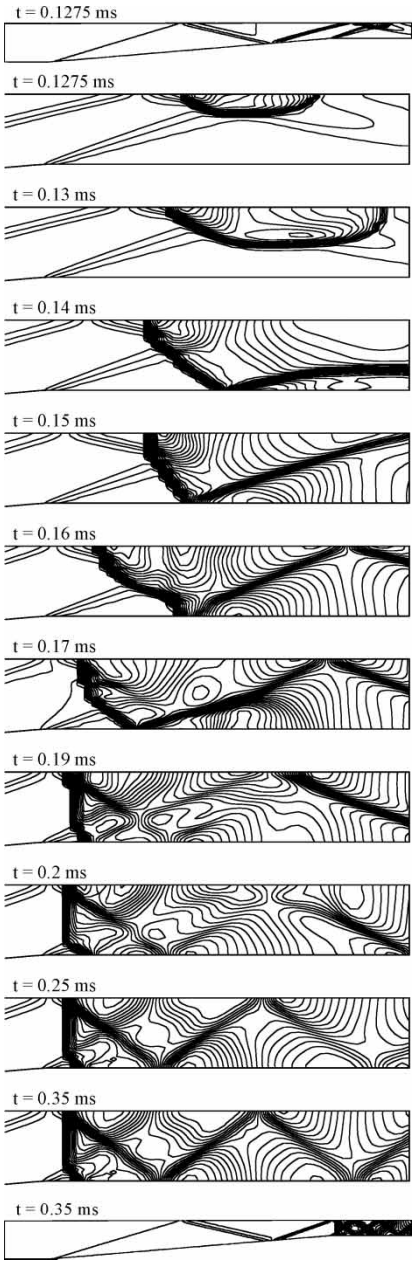

Fig. 10 Evolution of the SDW structure for $M_1 = 5$ and $\theta = 5°$; example case 1 of the SDW mode

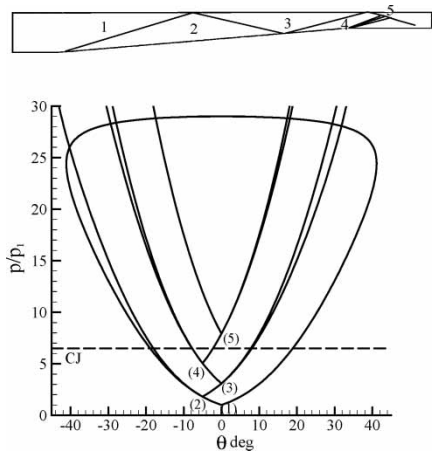

Fig. 11 Polar diagram for $M_1 = 5$ and $\theta = 5°$; example case 1 of the SDW mode

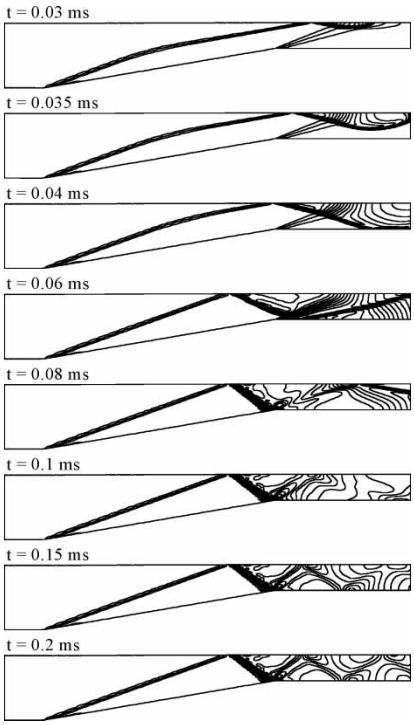

Fig. 12 Evolution of the SDW structure for $M_1 = 5.5$ and $\theta = 10°$; example case 2 of the SDW mode

the first two cases and on lower computational boundary for the third case in order to capture the detonation initiation process. As in the PDW mode, three time instances from the detonation initiation together with the instant just before detonation initiation are used to record the pressures for the first two cases and only three time instances from detonation initiation are used for the third case. The results in the figure show the narrow region with high thermodynamic parameters (in the figures, the pressures) arising from shock reflections that initiate the detonation. The detonation front strengths and the post-wave thermodynamic parameters are generally higher than the CJ state.

It is worthwhile to examine the wave structures obtained in the aftbody area for the SDW mode. From shock theory, oblique shocks cannot be maintained in a straight channel since no flow deflection boundary conditions exist in such a domain. Nonetheless, the results for the SDW mode show the presence of oblique wave reflection in the straight section (for example, in Figs 10, 12, and 14). Such a train of oblique shock waves can exist only in concert with a train of expansion waves originating from the opposite wall.

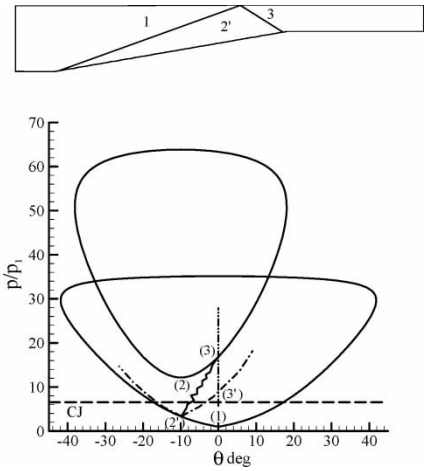

Fig. 13 Polar diagram for $M_1 = 5.5$ and $\theta = 10°$; example case 2 of the SDW mode

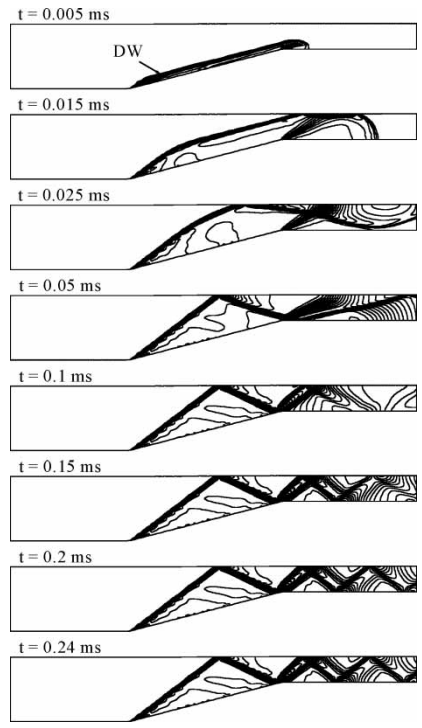

Fig. 14 Evolution of the SDW structure for $M_\infty = 6$ and $\theta = 15°$; example case 3 of the SDW mode

For this particular geometry, an oblique shock formed in the region downstream of the detonation front will encounter the expansion waves generated at the wedge shoulder and a mutual wave interaction is set up – the shock compresses the flow after it, whereas the expansion waves that keep in step with the shock then expands the flow. Since both of the waves are oblique, their alternate actions induce flow disturbances that propagate obliquely in the channel to eventually form the stabilized wave structures.

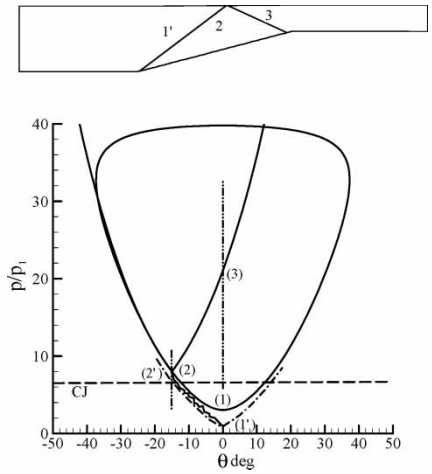

Fig. 15 Polar diagram for $M_1 = 6$ and $\theta = 15°$; example case 2 of the SDW mode

For a better view of the mutual interaction between opposite families of oblique shock and expansions, one of the three selected examples above was re-computed with the length of the aftbody elongated to three times the original. The stabilized pressure distribution for the elongated aftbody case is shown in Fig. 17 using a three-dimensional contour plot. The pressure peaks and valleys attain a regular pattern that arises from the mutual wave interaction. The figure also shows a decreasing tendency of the pressure fluctuation towards downstream as can be anticipated.

3.1.3 Non-detonative modes

For certain combinations of the input parameters M_1 and θ, particularly, for small θ, no detonation occurs. Instead, either a propagating or a standing shock, namely the PSW or the SSW mode, forms within the computational domain. An example of the PSW mode is shown in Fig. 18 via isobars for $M_1 = 1.5$ and $\theta = 10°$. The polar diagram for this case is depicted in Fig. 19, which suggests that the wedge-attached shock is unable to induce a regular flow reflection for the given deflection angle. In fact, the low value of the incoming Mach number causes the shock to be detached around the wedge and this results in unsteadiness in the confined channel flow. The numerical simulation for this case shows that the multiple wave reflections fail to stabilize in the channel. Disturbances that occur in the subsonic flow downstream propagate upstream, thereby causing the multiple waves to coalesce into the initial wedge-attached shock. Eventually, the wave coalescence produces a relatively strong normal shock which detaches rapidly, such that at $t = 0.625$ ms, and propagates out of the computational domain.

The pressure distribution along the lower computational boundary is shown in Fig. 20. The figure

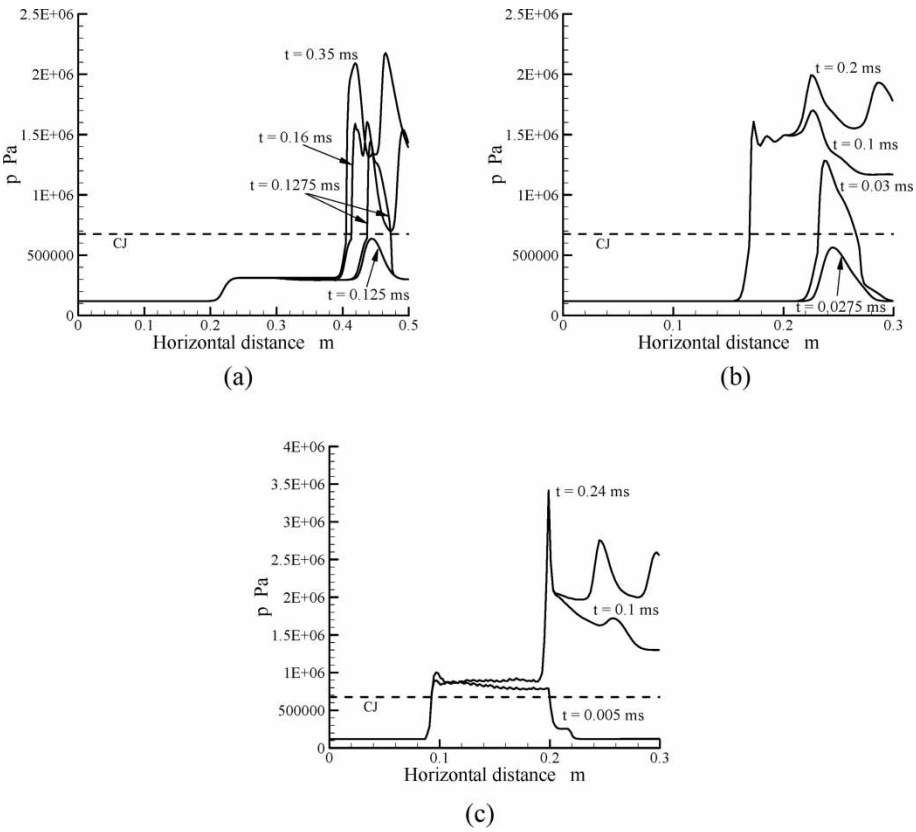

Fig. 16 Pressure distributions on the upper computation boundary, for example, case 1 ($M_1 = 5$, $\theta = 5°$) and case 2 ($M_1 = 5.5$, $\theta = 10°$) and on the lower computation boundary, for example, case 3 ($M_1 = 6$ and $\theta = 15°$) for the SDW mode

indicates a pressure rise at the wedge apex at $t = 0.005$ ms and an expansion at the wedge shoulder. The multiple shock reflections along the wedge surface are obviously expressed in the pressure distribution at $t = 0.4$ ms. The final distribution at $t = 0.625$ ms presents a strong pressure rise ahead of the wedge followed by a relatively flat plateau and a rapid drop at the shoulder. It can be seen that, despite compression from multiple shocks, the pressure does not approach the CJ level, leading to a non-detonative post-shock flow.

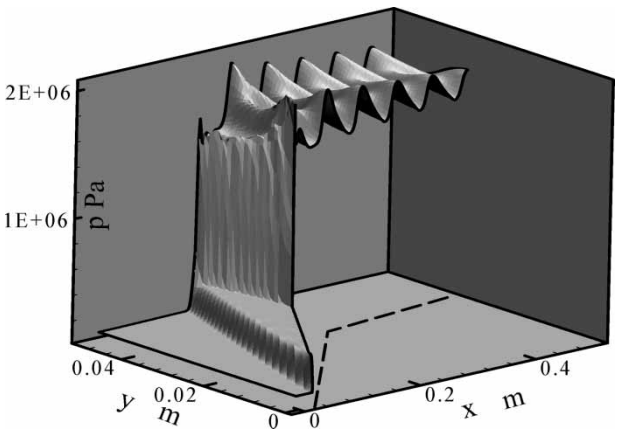

Fig. 17 Stabilized pressure distribution for $M_1 = 5.5$ and $\theta = 10$, an example case of the SDW mode

A stabilized, non-detonative mode occurs at higher Mach numbers while keeping the semi-angle small. An example of this SSW mode is shown in Fig. 21 for $M_1 = 5$ and $\theta = 2.5°$. The polar diagram for this case is plotted in Fig. 22. The numerical simulation for this case shows that the flow stabilizes with six standing oblique shocks in the channel. The stabilization process is also evident in the surface pressure distributions along the lower boundary, as shown in Fig. 23. The sequence of shock reflections resulting in distinct pressure jumps is obvious in this figure, reaching a steady state at $t = 0.45$ ms. The pressure stabilizes to a level below the CJ value (state 7 on the polar diagram) and, thus, no shock-induced detonation occurs within the computation domain.

Nevertheless, it can be easily shown that for the SSW mode, a long configuration can induce a sufficiently large number of wave reflections to cause the

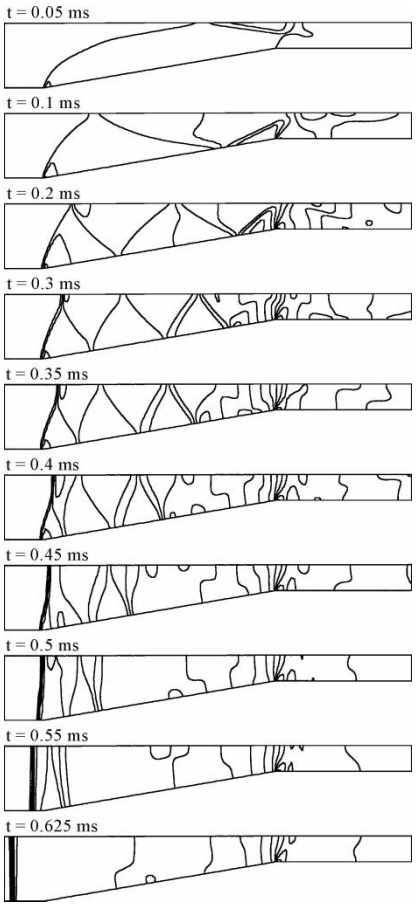

Fig. 18 Evolution of PSWs for $M_1 = 1.5$ and $\theta = 10°$; case of a PSW mode

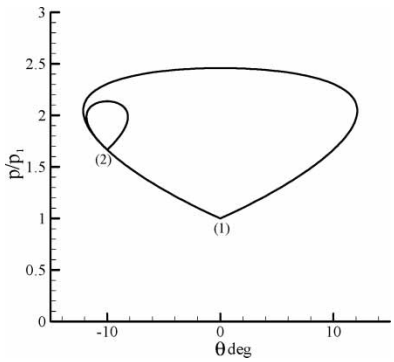

Fig. 19 Shock polar diagram for $M_1 = 1.5$ and $\theta = 10°$; example case of a PSW mode

pressure to exceed the CJ value, thereby inducing detonation. In the above example, from the polar diagram of Fig. 22, one can predict that two more reflections (states 8 and 9 on the dash-dotted polars) will bring the pressure to exceed the CJ value. Further simulations (not shown) also reveal that the increase in the number of reflection waves initiates detonation when the wedge is elongated while keeping other geometric parameters constant.

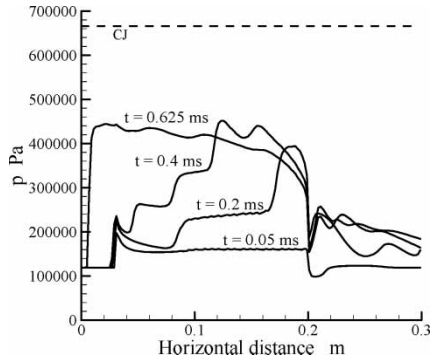

Fig. 20 Pressure distribution on the lower computational boundary for $M_1 = 1.5$, $\theta = 10°$; example case of an PSW mode

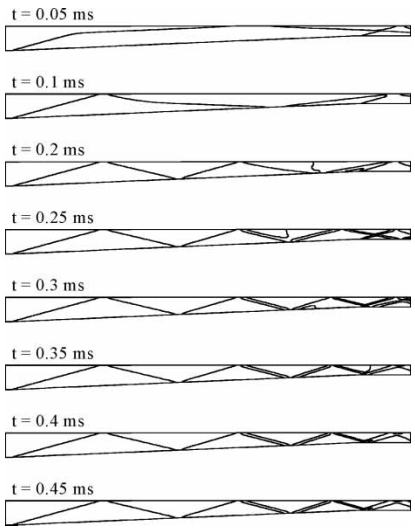

Fig. 21 Evolution of the SSWs structure for $M_1 = 5$ and $\theta = 2.5°$; example case of an SSW mode

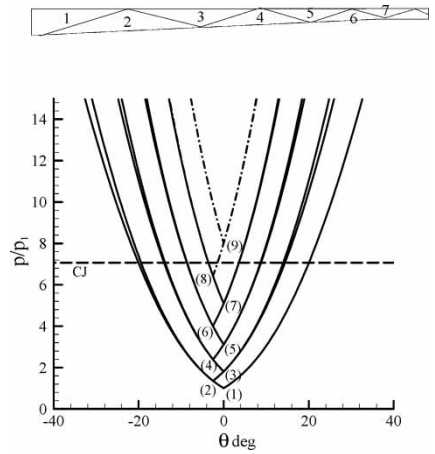

Fig. 22 Shock polar diagram for $M_1 = 5$ and $\theta = 2.5°$; example case of an SSW mode

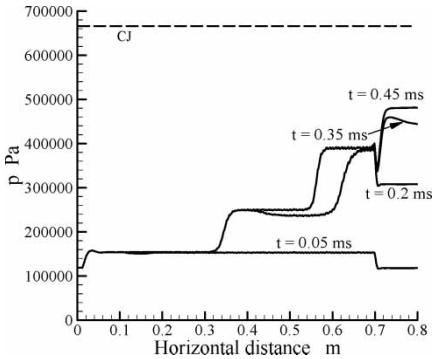

Fig. 23 Pressure distribution on the lower computational boundary for $M_1 = 5$, $\theta = 2.5°$; example case of an SSW mode

3.2 Further observations

3.2.1 Detonation waves induced by shock coalescence

The simulations reveal that detonation may not only be initiated by oblique shock reflections induced in the wedged channel but may also be induced by subsequent upstream-moving shocks. The latter situation usually occurs when (M_1, θ) are in the transitional region between the PSW and PDW modes (Fig. 2). In this situation, the shock waves at early time appear similar to those in the PSW mode, namely, multiple reflections following the wedge-attached shock. This shock system eventually results in a subsonic downstream flow that allows disturbances to propagate upstream, and hence causing multiple waves to coalesce with the initial wedge-attached shock. Unlike in the PSW mode, the coalescence of the shocks may induce a detonation wave.

Moreover, there appears to be two different possibilities for detonation initiation through shock coalescence. An example of detonation induced by shock coalescence is shown in Fig. 24 for the case of $M_1 = 1.5$ and $\theta = 12.5°$. Shock waves downstream of the wedge-attached shock propagate upstream and at $t = 0.5$ ms have coalesced to a relatively strong, normal shock. The strong shock at this time continues to propagate upstream to overtake the wedge-attached shock. When the shock passes over the wedge tip at about $t = 0.67$ ms, the flow is ignited at the vicinity of base of the coalesced shock front. The initiated detonation wave expands rapidly and propagates towards both ends of the channel.

The second possibility is presented in Fig. 25 for the case of $M_1 = 1.75$ and $\theta = 15°$. Here, shock waves after the wedge-attached shock coalesce with those upstream, eventually resulting in one strong λ shock. In Fig. 25, it can be seen that the wedge-attached shock begins to be deflected by the first reflected shock at $t = 0.3$ ms to yield a Mach reflection. The Mach stem impinging the upper surface increases in length

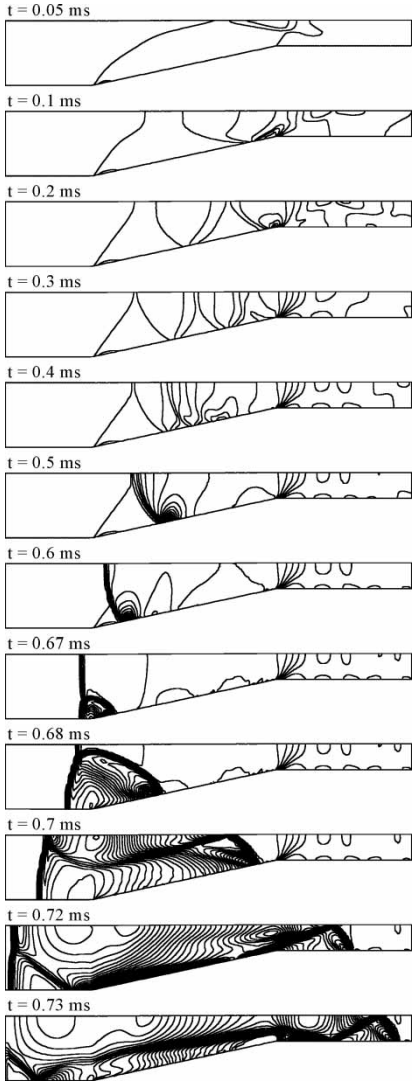

Fig. 24 Evolution of the PDWs induced by upstream-moving shock waves ($M_1 = 1.5$ and $\theta = 12.5°$, first possibility)

(and strength), and eventually detonation is ignited by the shock at its rear near the channel lower surface at about $t = 0.3875$ ms. Again, the detonation wave expands and propagates to the two ends of the channel.

3.2.2 Number of reflected shocks and location of detonation initiation

A classification scheme can be devised based on N, the total number of oblique shocks that exists before detonation initiation in either the PDW or SDW modes. For example, $N = 1$ indicates that detonation is initiated after a wedge-attached oblique shock impinges on the wall surface, and $N = 2$ means that detonation is initiated after two reflections and so on. In addition, $N = 0$ denotes that detonation is initiated directly after the wedge-attached oblique shock. The demarcations

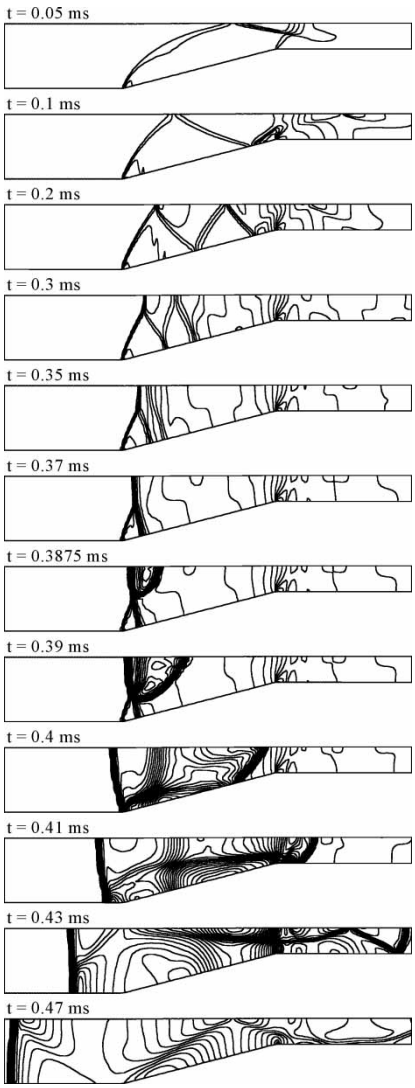

Fig. 25 Evolution of PDW induced by upstream-moving shock waves ($M_1 = 1.75$ and $\theta = 15°$, second possibility)

for $N = 0, 1$, and 2 are plotted in Fig. 2. Further, for the cases considered, N can reach up to 12. These values are indicated by small numerals adjacent to symbols.

The larger the incoming Mach number M_1 or the wedge semi-angle θ, the fewer shock reflections are needed for detonation to be ignited. Hence, the upper-right region in Fig. 2 is where detonation can occur directly from the wedge-induced shock. The following $N = 1, 2, \ldots, 12$ contours locate successively towards the lower-left corner of Fig. 2.

Detonation can be initiated from either the wall surface or the wedge-body surface of the considered channel. When M_1 and θ are given, the detonation initiation location is the surface on which a shock reflection first raises the pressure to the CJ value. Consequently, when N is odd, the initiation is from the wall surface while if N is 0 or even, detonation is initiated on the wedge-body surface.

3.2.3 λ-structure

In the PDW mode, if a propagating detonation front passes over the oblique shock reflections that are initiated from the wedge apex, a Mach reflection, λ-structure can appear. This phenomenon can be seen in Figs 3, 5, and 7. A more detailed discussion of this phenomenon is now given using Fig. 26 for two cases, namely, $M_1 = 3.5$, $\theta = 12.5°$ and $M_1 = 4.5$, $\theta = 20°$. In the figure, the λ-structure is presented at instants when the detonation front is over the wedge area, through isobars, isotherms, and isopycnics. The figures depict a wave structure formed by an upstream propagating normal detonation wave intersecting a stable oblique shock (or detonation) wave through a Mach stem. A contact discontinuity exists after the triple point that separates the fluid that has passed through the whole channel from the fluid that has passed only through the normal detonation wave. The contact discontinuity can be clearly seen in the temperature and density contours.

On the other hand, in the SDW mode, a detonation front encountering the expansion fan at the wedge shoulder is weakened and deflected so as to form a standing λ-foot. This phenomenon can also be clearly seen in the results of the previous three examples of the mode. Such λ-foot structures are further illustrated in detail in Fig. 27 for the cases of $\theta = 5°$ with $M_1 = 4.75$, 5.5, 5.25, and 5.5. From the results, it is obvious that the deflected part of the detonation front depends on the streamwise position where it is stabilized. The farther

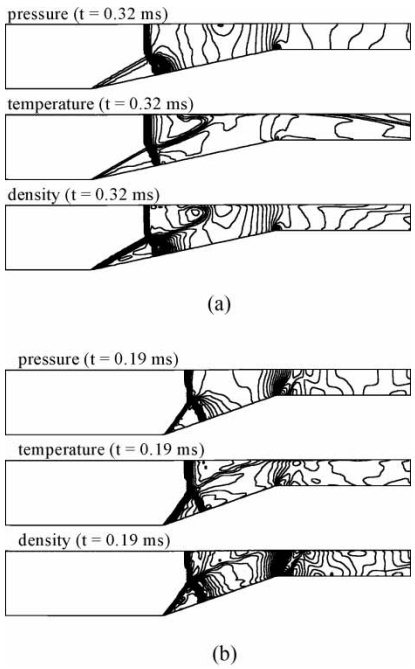

Fig. 26 Mach reflection λ-structure for two PDW cases: (a) $M_1 = 3.5$ and $\theta = 12.5°$; (b) $M_1 = 4.5$ and $\theta = 20°$

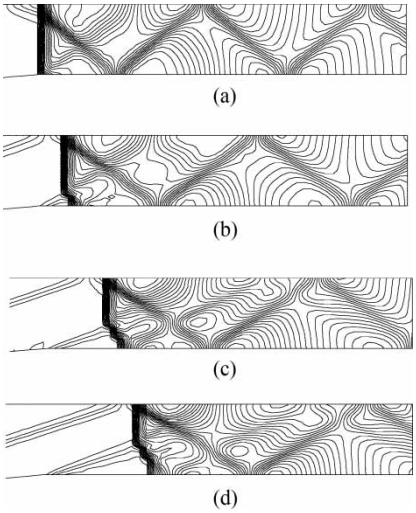

Fig. 27 Expansion fan λ-structure at four different M_1 with $\theta = 5°$ in the SDW mode: (a) $M_1 = 4.75$; (b) $M_1 = 5$; (c) $M_1 = 5.25$; (d) $M_1 = 5.5$

the detonation front is from the wedge shoulder, the larger the portion of the front that is influenced. Thus, Fig. 27(a) shows the case in which the detonation front is situated just before the wedge shoulder and consequently, it is not significantly affected by the expansion fan. However, Fig. 27(d) shows the case in which the detonation front is located rather far from the wedge shoulder and is thereby deflected most seriously by the expansion waves.

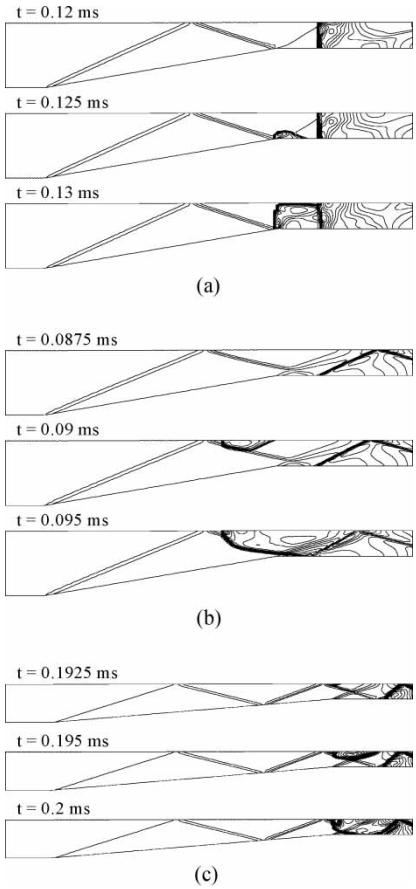

Fig. 28 Double detonation initiation phenomenon for three different cases: (a) $M_1 = 4$ and $\theta = 10°$; (b) $M_1 = 4.5$ and $\theta = 10°$; (c) $M_1 = 4.75$ and $\theta = 5°$

3.2.4 Double detonation initiation

In some cases, after detonation has been initiated and developed, a subsequent detonation kernel may still be triggered occasionally ahead of an existing detonation wave. This double detonation initiation phenomenon may arise in both the PDW and SDW modes. Three examples are shown in Fig. 28 with isobars to record the second detonation initiation processes. The first two cases belong to the PDW mode while the third is of the SDW mode. It can be seen that the second detonation initiation in each case starts in a tip area of an oblique shock ahead of the detonation wave. It is thought that the second detonation wave is excited by the strengthening of the upstream oblique shock from the upstream propagating detonation fronts. When a second detonation is initiated, it promptly expands to mix with the original detonation front to share the reactants in the small area between the two detonations. The mixing process forms a new complex detonation front that either propagates upstream or is stable.

4 CONCLUSIONS

The wedge-induced shock and detonation waves occurring in a two-dimensional symmetric wedged channel was studied numerically. A five-species and two-step reaction mechanism was adopted to model the thermo-chemical dynamics of the detonation processes and a time-accurate and finite-volume-based method was used to simulate the processes numerically. Semi-wedge angles of up to 20° were considered. The incoming Mach number was allowed to vary while the other inflow aerodynamic parameters were fixed. A qualitative understanding of the complex and rich shock and detonation flow was obtained. Emphases were paid on detonation phenomena. Different shock and detonation flow configurations were identified that are demonstrated to depend on the incoming Mach number and the wedge angle. In particular, four typical flow modes were presented that are classified based on the viewpoints whether the shock and detonation wave structure is propagating or standing and whether detonation occurs in the channel. Many flow

phenomena associated with the studied shock and detonation systems were presented and analysed.

REFERENCES

1 **Olejniczak, J., Wright, M. J.,** and **Candler, G. V.** Numerical study of inviscid shock interaction on the double-wedge geometries. *J. Fluid Mech.*, 1997, **325**, 1–25.

2 **Kumar, A.** Numerical simulation of flow through a two-strut scramjet inlet. *J. Propuls. Power*, 1989, **5**(3), 341–345.

3 **Tani, K., Kanda, T.,** and **Kudo, K.** Aerodynamic performance of scramjet inlet models with a single strut. *J. Propuls. Power*, 2006, **22**(4), 905–912.

4 **Reinartz, B. U., Herrmann, C. D., Ballmann, J.,** and **Koschel, W. W.** Aerodynamic performance analysis of a hypersonic inlet isolator using computation and experiment. *J. Propuls. Power*, 2003, **19**(5), 868–875.

5 **Kailasanath, K.** Review of propulsion applications of detonation waves. *AIAA J.*, 2000, **38**(9), 1698–1708.

6 **Munipalli, R., Shankar, V., Wilson, D. R., Kim, H., Lu, F. K.,** and **Hagseth, P. E.** A pulsed detonation based multimode engine concept. AIAA paper 2001-1786, 2001.

7 **Wilson, D. R., Lu, F. K., Kim, H.,** and **Munipalli, R.** Analysis of a pulsed normal detonation wave engine concept. AIAA paper 2001-1784, 2001.

8 **Sislian, J. P., Martens, R. P., Schwartzentruber, T. E.,** and **Parent, B.** Numerical simulation of a real shcramjet flowfield. *J. Propuls. Power,* 2006, **22**(5), 1039–1048.

9 **Grismer, M. J.** and **Powers, J. M.** Calculations for steady propagation of a generic ram accelerator configuration. *J. Propuls. Power*, 1995, **11**(1), 105–111.

10 **Lefebvre, M. H.** and **Fujiwara, T.** Numerical modeling of combustion processes induced by a supersonic conical blunt body. *Combust. Flame,* 1995, **100**(1–2), 85–93.

11 **Hertzberg, A., Bruckner, A. P.,** and **Bogdanoff, D. W.** Ram accelerator: a new chemical method for accelerating projectiles to ultrahigh velocities. *AIAA J.,* 1988, **26**(2), 195–203.

12 **Brackett, D. C.** and **Bogdanoff, D. W.** Computational investigation of oblique detonation ramjet-in-tube concepts. *J. Propuls. Power,* 1989, **5**(3), 276–281.

13 **Powers, J. M.** and **Stewart, D. S.** Approximate solution for oblique detonation in hypersonic limit. *AIAA J.*, 1992, **30**(3), 726–736.

14 **Terao, K., Ishii, K., Totsuka, T.,** and **Ishikawa, Y.** An experimental investigation of hypersonic combustion for ram jet engine applying detonation waves. AIAA paper 2002-5164, 2002.

15 **Lehr, H. F.** Experiments on shock-induced combustion. *Acta Astron.*, 1972, **17**, 58–597.

16 **Dabora, E. K., Desbordes, D., Guerraud, C.,** and **Wagner, H. G.** Oblique detonations at hyper velocities. *Prog. Astron. Aeron.*, 1991, **133**, 187–204.

17 **Desbordes, D., Hamada, L.,** and **Guerraud, C.** Supersonic H_2-air combustion behind oblique shock waves. *Shock Waves*, 1991, **4**(6), 339–345.

18 **Morris, C. I., Kamel, M. R., Stouklov, I. G.,** and **Hanson, R. K.** PLIF imagine of supersonic reactive flows around projectiles in an expansion tube. AIAA paper 96-0855, 1996.

19 **Guo, C., Zhang, D.,** and **Xie, W.** The Mach reflection of a detonation based on soot track measurements. *Combust. Flame*, 2001, **127**(3), 2051–2058.

20 **Arai, T., Masuda, S.,** and **Sakima, F.** Intake fuel injection and shock induced combustion in a scramjet engine model. AIAA paper 2003-6910, 2003.

21 **Fujiwara, T., Matsuo, A.,** and **Nomoto, H.** A two-dimensional detonation supported by a blunt body or a wedge. AIAA paper 88-0098, 1988.

22 **Cambier, J. L., Adelman, H. G.,** and **Menees, G. P.** Numerical simulations of oblique detonation waves in supersonic combustion chamber. *J. Propuls. Power*, 1989, **5**(4), 482–491.

23 **Li, C., Kailasanath, K.,** and **Oran, E. S.** Detonation structure behind oblique shocks. *Phys. Fluids*, 1994, **6**(4), 1600–1611.

24 **Grismer, M. J.** and **Powers, J. M.** Numerical prediction of oblique detonation stability boundaries. *Shock Waves*, 1996, **6**(3), 147–156.

25 **Yungster, S., Radhakrishnan, K.,** and **Rabinowitz, M. J.** Computational study of flow establishment in a ram accelerator. AIAA paper 95-2489, 1995.

26 **Gerlinger, P., Algermissen, J.,** and **Bruggemann, D.** Matrix dissipation for central difference scheme with combustion. *AIAA J.*, 1995, **33**(10), 1865–1870.

27 **Thaker, A. A.** and **Chelliah, H. K.** Numerical prediction of oblique detonation wave structures using detailed and reduced reaction mechanisms. *Combust. Theory Model.*, 1997, **1**(4), 347–376.

28 **Ohyagi, S., Obara, T., Nakata, F.,** and **Hoshi, S.** A numerical simulation of reflection processes of a detonation wave on a wedge. *Shock Waves*, 2000, **10**(3), 185–190.

29 **Figueira da Silva, L. F.** and **Deshaies, B.** Stabilization of an oblique detonation wave by a wedge: a parametric numerical study. *Combust. Flame*, 2000, **121**(1–2), 152–166.

30 **Papalexandris, M.** A numerical study of wedge-induced detonation. *Combust. Flame*, 2000, **120**(4), 526–538.

31 **Kim, H., Lu, F. K., Anderson, D. A.,** and **Wilson, D. R.** Numerical simulation of detonation process in a tube. *Comput. Fluid Dyn. J.*, 2003, **12**(2), 227–241.

32 **Millikan, R. C.** and **White, D. R.** Systematics of vibrational relaxation. *J. Chem. Phys.*, 1963, **39**(12), 3209–3213.

33 **Vincenti, W. G.** and **Kruger, C. H.** *Introduction to physical gas dynamics*, 1977 (Krieger, Malabar, Florida).

34 **Rogers, R. C.** and **Chinitz, W.** Using a global hydrogen-air combustion model in turbulent reacting flow calculations. *AIAA J.*, 1983, **21**(4), 586–592.

35 **Lu, F. K., Fan, H. Y.,** and **Wilson, D. R.** Detonation waves induced by a confined wedge. *Aerosp. Sci. Technol.*, 2006, **10**, 679–685.

36 **Lu, T., Law, C. K.,** and **Ju, Y.** Some aspects of chemical kinetics in Chapman-Jouguet detonation: induction length analysis. *J. Propuls., Power*, 2003, **19**(5), 901–907.

37 **Powers, J. M.** and **Paolucci, S.** Accurate spatial resolution estimates for reactive supersonic flow with detailed chemistry. *AIAA J.*, 2005, **43**(5), 1088–1099.

38 **Powers, J. M.** Review of multiscale modeling of detonation. *J. Propuls. Power*, 2006, **22**(6), 1217–1229.

39 **Fan, H. Y.** and **Lu, F. K.** Comparison study of detonation processes in a variable cross-section chamber and a simple tube. *J. Propuls. Power*, 2005, **21**(1), 65–75.

40 Lee, J. H. S. Initiation of gaseous detonation. *Annu. Rev. Phys. Chem.*, 1977, **28**, 75–104.

41 Lu, F. K. and **Wilson, D. R.** Detonation driver for enhancing shock tube performance. *Shock Waves*, 2003, **12**(6), 457–468.

42 Zucker, R. D. and **Biblarz, O.** *Fundamentals of gas dynamics*, 2002 (John Wiley & Sons, Inc., Hoboken, NJ).

43 Townend, L. H. An analysis of the oblique and normal detonation waves. Aeronautical Research Council R.&M. No. 3638, Her Majesty's Stationary Office, London, 1970.